

Geophysical Research Letters



RESEARCH LETTER

10.1029/2020GL091698

Key Points:

- First study to show the impacts of assimilating water isotopic observations in addition to conventional non-isotopic observations
- Assimilating water isotopes can produce additional improvements even when concurrent water vapor observations are assimilated
- Wind, humidity, and temperature fields can be improved by 3%–4% through unique isotopic effects

Supporting Information:

- Supporting Information S1

Correspondence to:

K. Toride,
kinya@iis.u-tokyo.ac.jp

Citation:

Toride, K., Yoshimura, K., Tada, M., Diekmann, C., Ertl, B., Khosrawi, F., & Schneider, M. (2021). Potential of mid-tropospheric water vapor isotopes to improve large-scale circulation and weather predictability. *Geophysical Research Letters*, 48, e2020GL091698. <https://doi.org/10.1029/2020GL091698>

Received 12 NOV 2020
 Accepted 12 FEB 2021

Potential of Mid-tropospheric Water Vapor Isotopes to Improve Large-Scale Circulation and Weather Predictability

Kinya Toride^{1,2} , Kei Yoshimura^{1,3} , Masataka Tada⁴, Christopher Diekmann⁵ , Benjamin Ertl^{5,6} , Farahnaz Khosrawi⁵ , and Matthias Schneider⁵

¹Institute of Industrial Science, The University of Tokyo, Chiba, Japan, ²Department of Atmospheric Sciences, University of Washington, Seattle, WA, USA, ³Earth Observation Research Center, Japan Aerospace Exploration Agency, Japan, ⁴Japan Weather Association, Tokyo, Japan, ⁵Institute of Meteorology and Climate Research, Karlsruhe Institute of Technology, Karlsruhe, Germany, ⁶Steinbuch Centre for Computing, Karlsruhe Institute of Technology, Karlsruhe, Germany

Abstract Recent satellite techniques have uncovered detailed tropospheric water vapor isotope patterns on a daily basis, yet the significance of water isotopes on weather forecasting has remained largely unknown. Here, we perform a proof-of-concept observing system simulation experiment to show that mid-tropospheric water isotopes observed by the Infrared Atmospheric Sounding Interferometer (IASI) can substantially improve weather forecasts through non-local impacts on the convective heating structure and large-scale circulation. Assimilating IASI isotopes can improve wind, humidity, and temperature fields by more than 10% at mid-troposphere compared to only assimilating conventional non-isotopic observations. These improvements are about two-thirds of assimilating simultaneous IASI water vapor observations. The improvements can be attributed more to thermodynamic (phase change) effects than dynamic (transport) effects of water isotopes. Furthermore, isotopic observations produce additional 3%–4% improvements to the fields constrained by the conventional observations and simultaneous IASI water vapor observations, demonstrating the unique characteristics of water isotopes.

Plain Language Summary Accurate weather forecasting has tremendous socio-economic benefits by saving lives from natural hazards and affecting numerous sectors including water resources, energy, and agriculture. Although recent satellite techniques have enabled observing detailed water isotope patterns (e.g., HDO and H₂¹⁸O) in the atmosphere, it has not been incorporated in operational weather forecasting. Here, we show that water isotopes can substantially improve weather forecasts by improving the heating structure and large-scale circulation. Satellite-observed isotopes can improve wind, humidity, and temperature fields up to 3%–4% compared to utilizing conventional non-isotopic observations and concurrent water vapor observations by the same satellite. We anticipate that our results will facilitate further modeling developments in isotopic processes and benefit the societal sectors by improving operational weather forecasting.

1. Introduction

Weather forecasting has steadily improved through better representation of physical processes, ensemble forecasting, and model initialization accompanied by increasing computing power and improved observational technology (Bauer et al., 2015). The accurate specification of initial conditions is crucial in the atmospheric system due to its nonlinear complexity or chaotic nature (Lorenz, 1963). The direct assimilation of satellite radiance data in addition to conventional observations has become the mainstream for initializing model conditions (Geer et al., 2018; Saunders et al., 2018), and recent studies have investigated the additional assimilation of atmospheric composition (Dai et al., 2019), ocean (Tardif et al., 2015), and land surface variables (Kotsuki, Miyoshi, et al., 2017; Sawada et al., 2018) to further advance model initialization. Among the additional variables, the isotopic composition of water has the potential to positively impact various meteorological variables by its unique constraints on hydrological processes (Yoshimura, 2015; Yoshimura et al., 2014).

© 2021. The Authors.

This is an open access article under the terms of the [Creative Commons Attribution License](https://creativecommons.org/licenses/by/4.0/), which permits use, distribution and reproduction in any medium, provided the original work is properly cited.

Stable water isotopes (e.g., HDO and H₂¹⁸O) are useful tracers in the hydrological cycle (Galewsky et al., 2016) due to the process called isotopic fractionation; when water vapor condenses, heavier isotopes preferentially condense more because of their greater binding energies and lower diffusive velocities (Craig, 1961; Dansgaard, 1964). Stable water isotopes in precipitation have been used to understand the hydrological cycle since the 1950s (Dansgaard, 1953, 1964). Recently, satellite remote sensing techniques have dramatically increased the number of tropospheric water vapor isotope observations (Frankenberg et al., 2009; Schneider et al., 2016, 2017; Worden et al., 2007), which hold more direct information of atmospheric processes than precipitation isotopes (Lacour et al., 2018). It is now possible to monitor daily tropospheric δD (the HDO abundance relative to the Vienna Standard Mean Ocean Water (VSMOW)) on a quasi-global scale from the Infrared Atmospheric Sounding Interferometer (IASI) on the Meteorological Operational satellite program (Metop; Schneider et al., 2016, 2017). Mid-tropospheric isotopes likely provide meaningful constraints to a data assimilation framework because the isotopes hold unique information about the history of water vapor due to the different signatures of mixing, Rayleigh-type rainout, and re-evaporation processes (Galewsky & Hurley, 2010; Noone, 2012; Yoshimura et al., 2011), which can also be used to deduce convective heating structure (Lacour et al., 2018). In spite of these increasing numbers of high-density δD observations and their potential, their significance on weather forecasting has been largely unexplored.

Here, we investigate the potential of mid-tropospheric δD to improve weather forecasting when operational conventional (non-isotopic) observations are already assimilated using an isotope-enabled general circulation model. We conduct idealized experiments, where the forecasting model is assumed to be perfect (see Text S1 and Figure S1 for more details), with synthetic IASI δD and paired water vapor (or H₂O) observations in addition to conventional observations. Through rigorous comparisons, we discover that the inclusion of δD improves atmospheric fields not only when conventional observations are assimilated but also when the concurrent water vapor observations are additionally assimilated. These results demonstrate the unique constraints of water vapor isotopes and mechanisms of the isotope assimilation impacts.

2. Materials and Methods

2.1. Model and Data Assimilation

We use the Isotope-incorporated Global Spectral Model (IsoGSM), which incorporates heavy water isotope tracers (HDO and H₂¹⁸O) as prognostic variables (Yoshimura et al., 2008). In this study, IsoGSM ensemble forecasts are performed with T62 horizontal resolution (about 180 km) and 28 vertical sigma levels. IsoGSM simulations have been validated by ground-based isotopic measurements (Schneider et al., 2010; Uemura et al., 2008) and satellite observations (Frankenberg et al., 2009; Yoshimura et al., 2011). The sea surface temperature and sea ice distribution used in the National Centers for Environmental Prediction/Department of Energy Reanalysis 2 (NCEP-DOE Reanalysis 2) are used as lower boundary conditions.

The local ensemble transform Kalman filter (LETKF) (Hunt et al., 2007), a parallel-efficient upgrade of the traditional ensemble Kalman filter (EnKF), is employed in this study as an assimilation technique. The model state used in LETKF includes horizontal wind speeds, temperature, specific humidity, water isotope ratios (δD and δ¹⁸O), surface pressure, and precipitation. Here δD and δ¹⁸O are converted from the mixing ratios of HDO and H₂¹⁸O simulated by IsoGSM. The observations are assimilated every 6-h. The ensemble size of 96 is chosen based on the results with different ensemble sizes as shown in Figure S2. We employ the relaxation to prior spread method (Whitaker & Hamill, 2012) with the relaxation parameter of 0.4. Other covariance inflation methods including a constant multiplicative method and adaptive method (Miyoshi, 2011) show similar results but exhibit relatively unstable isotopic behavior in the stratosphere (not shown). The horizontal localization scale is selected to be 500 km (the influence radius of 1,826 km) for best assimilation performance (Figure S3). See Text S2 for further details on data assimilation.

2.2. Data

We mock the characteristics of the IASI δD and H₂O pair observations generated by the MUSICA IASI retrieval processor (Schneider et al., 2016, 2017). The real IASI data set provides the δD and H₂O pair distribution twice per day on a quasi-global scale (about 300,000 points) with 11 vertical layers from 1.3 to 8.0 km height. The global MUSICA IASI {H₂O, δD} pair product is becoming available by the end of February

2021 at <http://www.imk-asf.kit.edu/english/musica-iasi-h2oiso-v2.php>. To generate synthetic IASI data, we identify the spatial coverage and observational error statistics using the real IASI observations. We only select the data fulfilling high sensitivity requirements in order to avoid the usage of averaging kernels (i.e., observations at 4.2 km, observations over the land with low surface roughness, water surface, or sea ice surface, cloud-free or small cloud cover, high quality, high vertical resolution, and high retrieval response). The data are spatially resampled to the IsoGSM grid points at one vertical level (σ level of 0.568) and missing values are assigned for the grid points where the number of effective IASI observations is less than 10. The observational error variances (σ_o^2) of IASI are estimated as the sum of spatial representative error variance (σ_s^2) and instrumental error variance (σ_i^2) (Zhang et al., 2008). These characteristics are used to generate synthetic observations from IsoGSM simulation. Similarly, the synthetic conventional observations (radiosondes, wind profilers, aircrafts, ships, buoys, surface stations, and wind data derived from satellites and radar) are generated based on the data set used in the NCEP operational system (known as PREPBUFR). PREPBUFR is a well-used data set in data assimilation studies for benchmark assessments (i.e., Kotsuki, Ota, & Miyoshi, 2017; Miyoshi et al., 2015; Torn, 2010). The conventional observations are also spatially resampled to the IsoGSM grid points. The average numbers of assimilated observations per day are 541,602 for conventional observations and 11,317 for IASI (2.1% of conventional observations). The spatial distributions of assimilated observations are shown in Figures S4 and S5.

2.3. Experimental Design

Four observation system simulation experiments (OSSEs) with 96 ensemble members are conducted to investigate the potential impacts of assimilating IASI water vapor isotopic observations. OSSEs are benchmark experiments where model-generated synthetic observations are used instead of actual observations to evaluate the added value of the observations (Text S1 and Figure S1). The synthetic conventional observations are assimilated in all experiments. The control OSSE is the reference only assimilating the conventional observations (CTRL). The second and third experiments additionally assimilate synthetic IASI δD and H_2O observations, respectively (IASI- δD and IASI-q). The last experiment assimilates both IASI δD and H_2O observations in addition to the conventional observations (IASI-q- δD). Table S1 summarizes the assimilated variables in each experiment. The nature run is generated by simulating the IsoGSM for 2 years initiated at 0000 UTC June 1, 2015. The first year is discarded as a spin-up period to minimize the possibility of the model's drift, and the two-month from July 1, 2016 to September 1, 2016 is selected as the experimental period. The initial conditions for 96 ensemble members are chosen from the nature run from 0000 UTC June 1, 2016 with a 6-h time step so that the initial conditions can be considered independent of the nature run but include similar climatological conditions. The synthetic observations are generated by adding Gaussian noises with given error statistics to the nature run. The results of the four experiments are evaluated in the latter one-month period from August 1, 2016 to September 1, 2016.

We also investigate the impacts of assimilating IASI δD data on forecasts. We conduct 5-day (120 h) free ensemble forecasts based on every 2-day ensemble mean analysis in August 2016 (i.e., 0000 UTC on August 1, 3, 5, ..., 31, 2016) for the four experiments. The mean behavior and statistical significance are estimated based on each of 16 forecasting experiments from different initial conditions.

Furthermore, additional experiments to investigate the impacts of dynamic and thermodynamic processes are conducted using the variable localization method (Kang et al., 2011). These experiments are designed similar to the IASI- δD experiment except zeroing out covariances between δD and specific humidity/temperature (Dynamic experiment), and δD and horizontal winds (Thermodynamic experiment) when δD is assimilated. Note that this is a one-way localization. The covariances are not modified when other variables are assimilated so that the impacts of conventional observations are maintained. See Text S2 and Figure S6 for further details.

The results are evaluated based on the 6-h root-mean-square error (RMSE) between each experiment's ensemble mean and the nature run and RMSE skill. The RMSE skill (%) is defined by

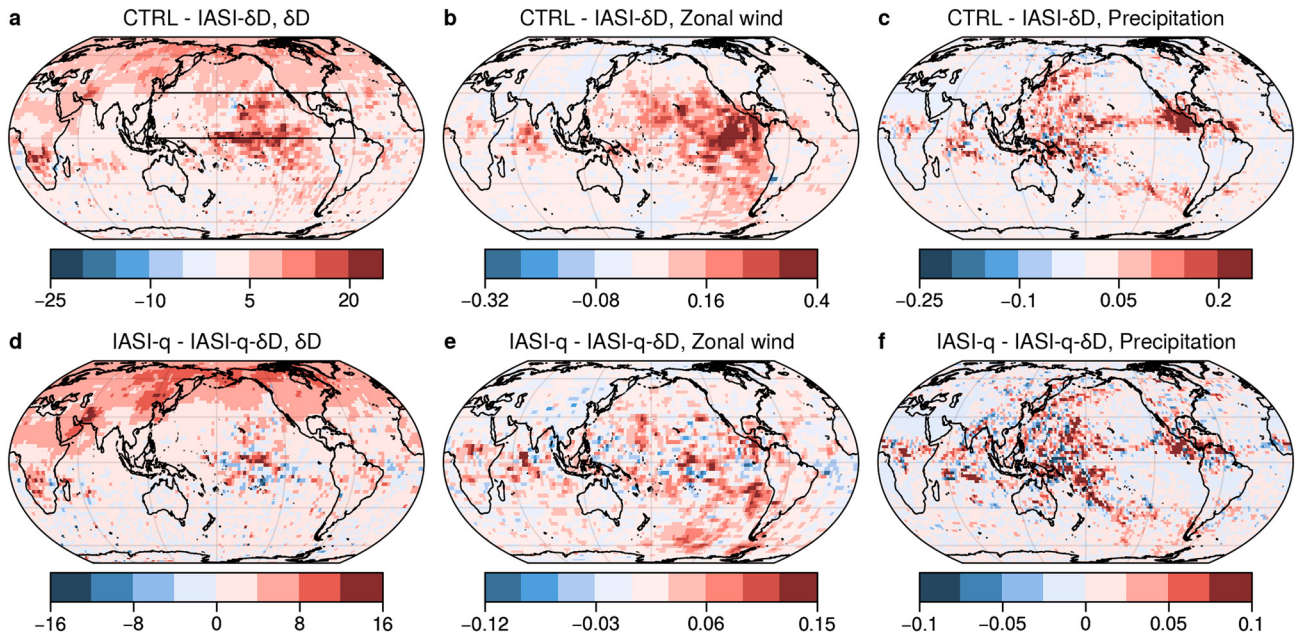


Figure 1. Improvements by the IASI δD assimilation. Spatial patterns of the changes in RMSEs between the CTRL and IASI- δD experiments in terms of (a) 500 hPa δD ($\%$), (b) 500 hPa zonal wind (m s^{-1}), and (c) precipitation (mm 6 h^{-1}) over 1 month from August 1, 2016 to August 31, 2016. (d)–(f) As in (a)–(c) but for the IASI-q and IASI-q- δD experiments. The red and blue colors represent improvement and degradation in RMSEs due to the water isotope data assimilation, respectively. IASI, Infrared Atmospheric Sounding Interferometer; RMSE, root-mean-square error.

$$\text{RMSE skill} = \frac{\text{RMSE}_{\text{CTRL}} - \text{RMSE}}{\text{RMSE}_{\text{CTRL}}} \times 100$$

where $\text{RMSE}_{\text{CTRL}}$ is the RMSE of the baseline CTRL experiment. Positive values indicate improvements from CTRL. The uncertainty ranges and statistical significance are evaluated as provided in Text S3.

3. Results

3.1. Assimilation of IASI δD Observations

Here, we first compare CTRL and IASI- δD to demonstrate the useful information of isotopes. Figure 1 shows the geographical patterns of the changes in RMSE by the water isotope assimilation. The IASI- δD experiment exhibits notable improvements in all variables, indicating the positive impacts of water vapor isotopes (Figures 1a–1c). δD is improved nearly globally with the spatial pattern following the locations of conventional and IASI observations (Figure S4); greater improvements are seen at low latitude, especially over the tropical Pacific (Figure 1a). The improvements in the zonal wind are concentrated on the east side of the δD improved regions, where the conventional observations are limited (Figure 1b). This indicates that the δD assimilation compensates for deficits in conventional observations. Temperature and specific humidity have analogous improvement patterns with larger improvements over the southwest Pacific. Improvements in precipitation are also similar and strongest over the raising branches in the Walker circulation (Figure 1c).

Although Figures 1a–1c illustrates the added values of δD compared to the conventional observations, larger improvements can be obtained from assimilating concurrent IASI H_2O observations because water vapor holds more direct relationships with other atmospheric variables. Figures 1d–1f shows the impacts of assimilating IASI $\{\text{H}_2\text{O}, \delta D\}$ pair observations compared to assimilating IASI H_2O observations, demonstrating if δD possesses any additional information. The improvements in δD are mostly in higher latitude in the northern hemisphere (Figure 1d). This is likely because the δD assimilation removes biases caused by the concentrated conventional observations in the northern hemisphere (Figure S4). The primary improvement

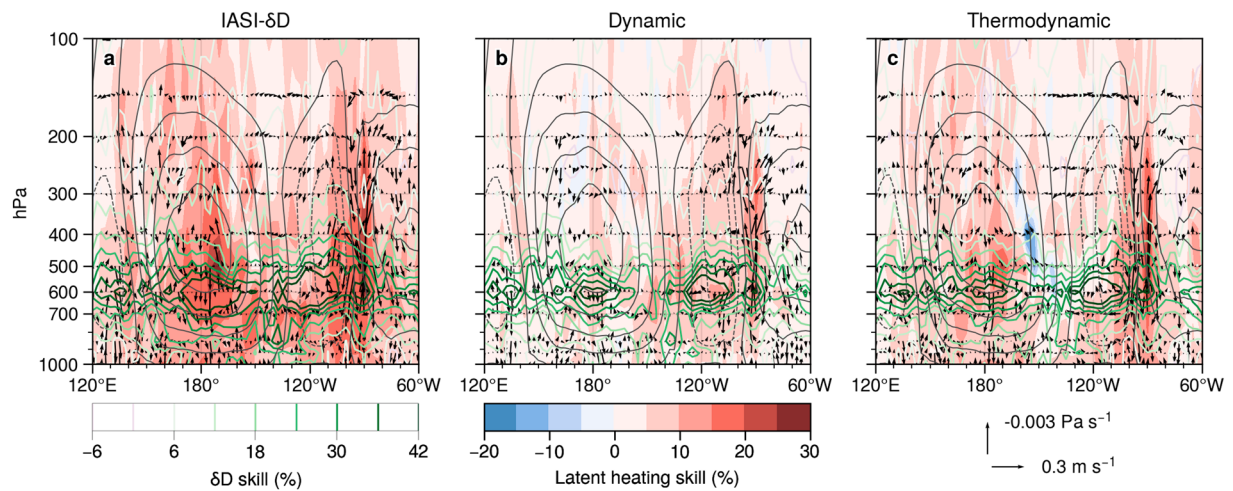


Figure 2. Non-local impacts on the structure of latent heating and large-scale circulation. (a) IASI- δD ; (b) Dynamic; (c) Thermodynamic experiments. The shading and colored contours show the RMSE skill (%) in latent heating and δD compared to the CTRL experiment, respectively. The vector shows the mean difference in vertical and zonal wind fields compared to the CTRL experiment. The gray contour represents the zonal mass stream function (10^9 kg s^{-1} interval). The values are averaged over the 0° – 30°N region, shown in Figure 1. IASI, Infrared Atmospheric Sounding Interferometer; RMSE, root-mean-square error.

region over the tropical Pacific seen in Figure 1a is weakened in the IASI- q - δD experiment. The improvements in wind and precipitation fields are not as robust as those in IASI- δD but are overall positive centered around the southeast Pacific and the tropical regions.

Stable water isotopes are known to be related to the depth and intensity of convective activity (Lacour et al., 2018; Torri et al., 2017). Figure 2 shows the assimilation impacts on the latent heating profile over the tropics for IASI- δD (see Text S4 for the calculation process). While larger improvements in δD are seen at the 600 hPa level where δD observations are located, latent heating results show improvements throughout the troposphere, demonstrating the non-local impacts of δD assimilation (Figure 2a). The significant improvements are observed in the enhanced convective activity regions around 140°E and 90°W , where the impacts on heating are vertically transported to the upper troposphere through the Walker circulation. Another large improvement region is located in the center of the circulation around 170°W . In contrast, smaller impacts are observed in the descending branch of the overturning cell (around 140°W), indicating that the assimilation effects can be limited at regions where phase changes occur less frequently. The δD assimilation also impacts the mean circulation; for instance, upwelling motions around 90°W are shifted toward the east. Hence, both dynamic and thermodynamic fields are improved by the mid-tropospheric δD assimilation. The IASI- q results (not shown) exhibit similar and stronger improvements than IASI- δD . Because water vapor and water vapor isotopes are closely related variables, it suggests that the δD assimilation is also benefitting from the relationship between moisture and convection (e.g., Brown & Zhang, 1997; Takemi et al., 2004).

Water vapor isotopes are passive tracers in the atmosphere distributed by transport/mixing (dynamic) and phase change (thermodynamic) processes. Here, additional experiments are conducted to address which process is dominant using the variable localization technique (Kang et al., 2011). We modify the covariance of prior ensembles so that the δD assimilation does not impact specific humidity and temperature (Dynamic experiment), or zonal and meridional wind (Thermodynamic experiment). Note that this is not a perfect separation of the two processes because the separation is only limited in data assimilation and atmospheric fields can be indirectly modified through the ensemble forecasts of priors by the general circulation model. Figures 2b and 2c show that the mean circulation in the Dynamic and Thermodynamic experiment is similarly modified as the IASI- δD experiment, particularly at the rising branch around 90°W . Still, the Thermodynamic experiment shows more substantial impacts on latent heating throughout the troposphere. The thermodynamic effect alone, however, may not be sufficient as can be seen from the deterioration in the downwelling branch in the Thermodynamic experiments. Overall, results indicate the dominance of

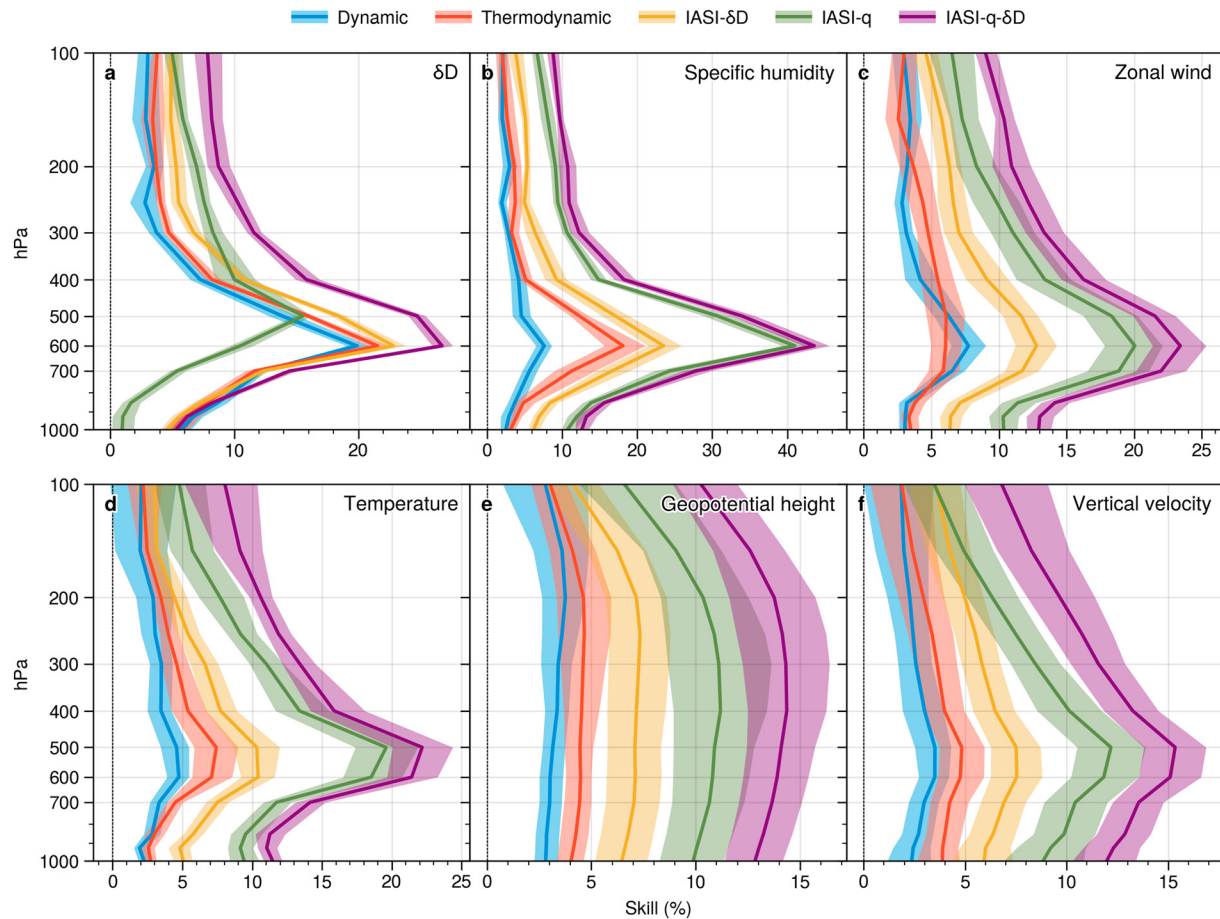


Figure 3. Improvement profiles by the IASI δD and q assimilation compared to CTRL. Profiles of global RMSE skills (%) over 1 month from August 1, 2016 to August 31, 2016 in terms of (a) δD , (b) specific humidity, (c) zonal wind, (d) temperature, (e) geopotential height, and (f) vertical velocity for the Dynamic, Thermodynamic, IASI- δD , IASI- q , and IASI- q - δD experiments. Shading shows the 95% confidence interval according to the bootstrap algorithm. IASI, Infrared Atmospheric Sounding Interferometer; RMSE, root-mean-square error.

the thermodynamic effect in isotopic data assimilation. This tendency is also consistent in the IASI- q - δD experiment (Text S5 and Figure S7).

The improvement profiles over the troposphere are depicted for various variables in Figure 3 compared to CTRL. The robust role of mid-tropospheric δD is clearly described as all variables are significantly improved throughout the troposphere. The peaks of improvements by the δD assimilation are seen around 600 hPa, where the improvements are >20% for δD and specific humidity, >10% for zonal wind and temperature, and 7% for geopotential height and vertical velocity. Note that geopotential height and vertical velocity are not included in the assimilation state vector. The Thermodynamic experiment outperforms the Dynamic experiment except for zonal wind around 600 hPa. The Thermodynamic experiment shows the larger indirect impacts on the zonal wind at other layers than the direct impacts in the Dynamic experiment.

A previous study showed that water isotopes assimilation improved temperature more than horizontal wind due to the stronger relationship between air temperature and the isotopic ratio through Rayleigh distillation (Yoshimura et al., 2014). However, in our experiment, stronger impacts are seen in the dynamics (i.e., wind field). This is because in this study, the atmospheric state is already well-constrained by conventional observations, and the impacts reflect the places with room for additional improvements. Furthermore, the improvements by assimilating water vapor isotopes are in general larger than those of the previous study (Yoshimura et al., 2014). The greater improvements are the results of the relatively large ensemble size chosen in this study as shown in Figure S2 (ensemble size of 20 is used in the previous study). The 96 ensemble

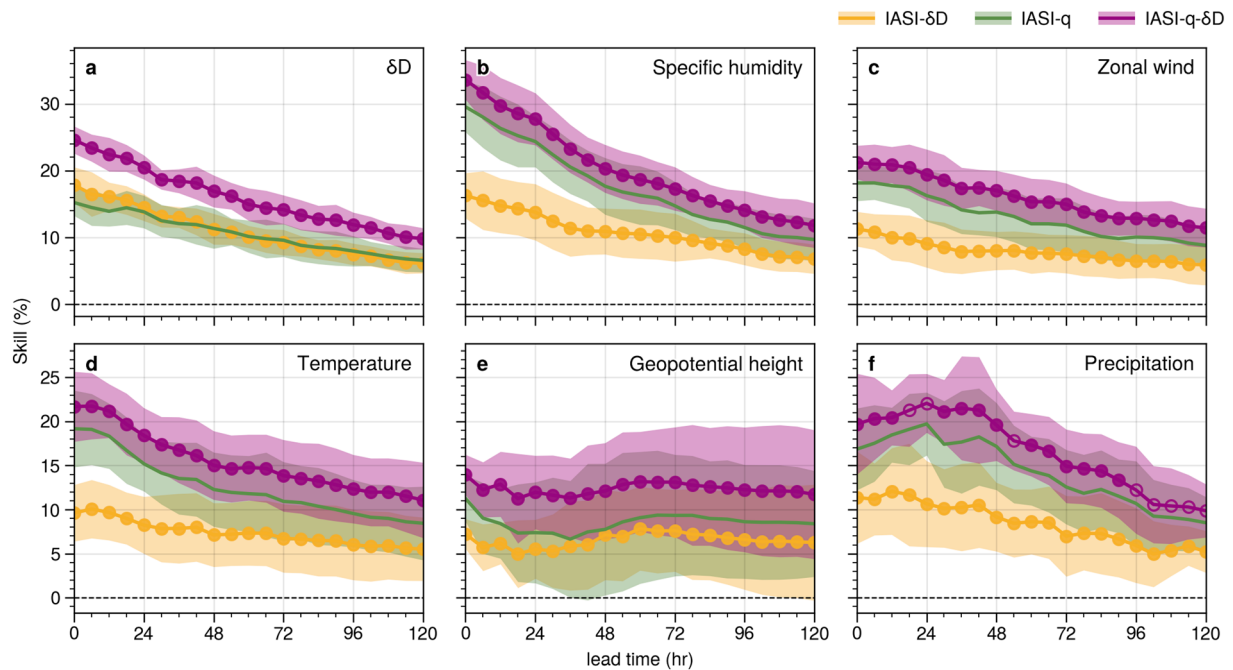


Figure 4. Improvements in forecast skills by the IASI δ D and q assimilation. Time series of global RMSE skills over 16 forecasting experiments (line; mean, shading; 1 σ) in terms of (a) δ D, (b) specific humidity, (c) zonal wind, (d) temperature, (e) geopotential height at 500 hPa, and (f) precipitation, for the IASI- δ D, IASI-q, and IASI-q- δ D experiments. The one-sided permutation tests are conducted between the CTRL and IASI- δ D experiments, and the IASI-q and IASI-q- δ D experiments to examine the improvements. All tests show statistical significance at the 5% level. The circles are filled when the significance level is 1%. IASI, Infrared Atmospheric Sounding Interferometer; RMSE, root-mean-square error.

members reduce sampling errors in the ensemble correlations between the isotopic ratio and various atmospheric variables (Figure S3).

Figure 3 summarizes RMSE improvements for the experiments assimilating IASI H₂O observations (IASI-q) and assimilating both IASI δ D and H₂O observations (IASI-q- δ D) in addition to the conventional observations. In general, IASI-q has greater improvements than IASI- δ D except for δ D. This is expected because IASI δ D and H₂O observations are assimilated with the same geographical distribution and temporal frequency, and water vapor has tighter direct connections with atmospheric dynamics and thermodynamics than δ D. The improvements by assimilating water vapor are 31% in specific humidity, and around 18% in wind speed, temperature at 500 hPa. Although conventional observations also contain specific humidity, the better spatial coverage of IASI around 600 hPa (Figure S5) results in the substantial improvements. Overall, the assimilation impacts of δ D are about 50%–70% of those of water vapor for non-isotopic variables, but δ D itself is in general better constrained by the δ D assimilation.

Another important aspect is the difference between the IASI-q and IASI-q- δ D experiments. It shows whether δ D has additional impacts on the fields already constrained by the water vapor observations, highlighting the unique characteristics of δ D. Figure 3 shows that greater improvements are made in IASI-q- δ D for all variables than in IASI-q. As changes in δ D due to air parcel mixing are different from the changes due to Rayleigh distillation at the same specific humidity (Galewsky & Hurley, 2010; Noone, 2012; Yoshimura et al., 2011), these results confirm that water isotopes hold different aspects of information than water vapor. All non-isotopic variables are improved additionally by around 3%–4% at mid-troposphere than the IASI-q experiment. Further details on IASI-q- δ D improvements relative to IASI-q are provided in Text S5 and Figures S7–S9.

3.2. Impacts on Weather Forecasting

Forecasting skills of key variables are analyzed at 500 hPa up to 120-h based on the 16 ensemble forecast experiments from different initial conditions (Figure 4). A permutation test shows that the forecast skills

are statistically improved in IASI- δD at a significance level of 1% throughout the 120-h forecasting period for all variables. The forecasting skill of specific humidity is improved by 10% up to 72-h and by 8% up to 120-h, and that of precipitation is also improved by 5% up to 120-h by the assimilation of δD . The IASI-q- δD experiment shows that δD assimilation in addition to the concurrent H₂O observations further improves the forecasting skills with statistical significance up to 120-h for all variables (also shown in Figure S9). These results again confirm the unique and effective information that water vapor isotopes possess.

4. Conclusions

In this study, the potential impacts of water vapor isotope assimilation are investigated using synthetic high-resolution IASI observations at the mid-troposphere. As hypothesized by previous studies (Galewsky & Hurley, 2010; Noone, 2012; Yoshimura et al., 2011), the mid-tropospheric water isotopes hold useful information and significantly contribute to constraining atmospheric fields. The assimilation of IASI δD in addition to conventional observations improves the analysis of wind, moisture, temperature, geopotential height, and latent heating fields throughout the troposphere. Geographically, larger improvements are seen in lower latitudes and the central and southeast Pacific. Forecasting experiments demonstrate that better initial conditions obtained by the δD assimilation can statistically improve forecast skills particularly for wind and humidity for 120-h. Moreover, the quantitative role of the water vapor isotope is examined relative to the assimilation impacts of concurrent water vapor observations. The results show that the assimilation impacts of IASI δD are about two-thirds of those of IASI water vapor. We also demonstrate that IASI δD can produce additional 3%–4% improvements to the fields constrained by the conventional observations and simultaneous IASI water vapor observations. This result highlights that water isotopes hold different aspects of information than water vapor.

While we examine the potential impacts of IASI water vapor isotope observation on weather analysis and forecasts relative to using conventional observations only, there may remain several uncertainties in assimilating real IASI observations. These uncertainties are inherent to water isotope modeling and observations such as systematic biases (i.e., underestimated latitudinal gradient in water vapor isotope) in isotope-enabled atmospheric models (Risi et al., 2012; Yoshimura et al., 2011) possibly due to the limitations in convective mixing and cloud processes in the tropical troposphere in climate models (Bony et al., 2015; Sherwood et al., 2014). Furthermore, the atmospheric state-dependent vertical information of the IASI data has to be considered for correctly assimilating the IASI observations (an observation operator is needed (Schneider et al., 2017)). Despite these practical considerations, we anticipate that the significance of water vapor isotopes demonstrated in the current study will further facilitate developments in modeling and observing isotopic processes. We envision that the inclusion of water vapor isotopes will become a mainstream practice for the weather forecasting industry worldwide and will significantly improve the weather forecasting accuracy on a global scale.

Acknowledgments

The authors thank G. Hakim, P. Blossey, and Y. Shi for discussions and suggestions. Comments by J. Galewsky and one anonymous reviewer are very beneficial. This work was supported by JSPS KAKENHI Grant 19J01337, 18H03794, and 16H06291, and JRP-LEAD with DFG, and the Integrated Research Program for Advancing Climate Models (TOUGOU) Grant Number JPMXD0717935457, ArCS II (Program Grant Number JPMXD1420318865), and DIAS from the Ministry of Education, Culture, Sports, Science and Technology (MEXT), Japan. The authors acknowledge funds of the DFG (provided for the two projects MOTIV and TEDDY with IDs/Geschäftszeichen 290612604GZ:SCHN1126/2-1 and 416767181/GZ:SCHN1126/5-1, respectively). The MUSICA IASI processing is performed on the supercomputer ForHLR funded by the Ministry of Science, Research and the Arts Baden-Württemberg and by the German Federal Ministry of Education and Research.

Data Availability Statement

The experimental results can be found online (<https://doi.org/10.5281/zenodo.4420315>).

References

- Bauer, P., Thorpe, A., & Brunet, G. (2015). The quiet revolution of numerical weather prediction. *Nature*, 525(7567), 47–55. <https://doi.org/10.1038/nature14956>
- Bony, S., Stevens, B., Frierson, D. M. W., Jakob, C., Kageyama, M., Pincus, R., et al. (2015). Clouds, circulation and climate sensitivity. *Nature Geoscience*, 8(4), 261–268. <https://doi.org/10.1038/ngeo2398>
- Brown, R. G., & Zhang, C. (1997). Variability of midtropospheric moisture and its effect on cloud-top height distribution during TOGA COARE*. *Journal of the Atmospheric Sciences*, 54(23), 2760–2774. [https://doi.org/10.1175/1520-0469\(1997\)054<2760:VOMMAI>2.0.CO;2](https://doi.org/10.1175/1520-0469(1997)054<2760:VOMMAI>2.0.CO;2)
- Craig, H. (1961). Isotopic variations in meteoric waters. *Science*, 133(3465), 1702–1703. <https://doi.org/10.1126/science.133.3465.1702>
- Dai, T., Cheng, Y., Suzuki, K., Goto, D., Kikuchi, M., Schutgens, N. A. J., et al. (2019). Hourly aerosol assimilation of Himawari-8 AOT using the four-dimensional local ensemble transform kalman filter. *Journal of Advances in Modeling Earth Systems*, 11(3), 680–711. <https://doi.org/10.1029/2018MS001475>
- Dansgaard, W. (1953). The abundance of O 18 in atmospheric water and water vapor. *Tellus*, 5(4), 461–469. <https://doi.org/10.1111/j.2153-3490.1953.tb01076.x>
- Dansgaard, W. (1964). Stable isotopes in precipitation. *Tellus*, 16(4), 436–468. <https://doi.org/10.3402/tellusa.v16i4.8993>

- Frankenberg, C., Yoshimura, K., Warneke, T., Aben, I., Butz, A., Deutscher, N., et al. (2009). Dynamic processes governing lower-tropospheric HDO/H₂O ratios as observed from space and ground. *Science*, 325(5946), 1374–1377. <https://doi.org/10.1126/science.1173791>
- Galewsky, J., & Hurlley, J. V. (2010). An advection-condensation model for subtropical water vapor isotopic ratios. *Journal of Geophysical Research*, 115(D16), D16116. <https://doi.org/10.1029/2009JD013651>
- Galewsky, J., Steen-Larsen, H. C., Field, R. D., Worden, J., Risi, C., & Schneider, M. (2016). Stable isotopes in atmospheric water vapor and applications to the hydrologic cycle. *Reviews of Geophysics*, 54(4), 809–865. <https://doi.org/10.1002/2015RG000512>
- Geer, A. J., Lonitz, K., Weston, P., Kazumori, M., Okamoto, K., Zhu, Y., et al. (2018). All-sky satellite data assimilation at operational weather forecasting centers. *Quarterly Journal of the Royal Meteorological Society*, 144(713), 1191–1217. <https://doi.org/10.1002/qj.3202>
- Hunt, B. R., Kostelich, E. J., & Szunyogh, I. (2007). Efficient data assimilation for spatiotemporal chaos: A local ensemble transform Kalman filter. *Physica D: Nonlinear Phenomena*, 230(1–2), 112–126. <https://doi.org/10.1016/j.physd.2006.11.008>
- Kang, J.-S., Kalnay, E., Liu, J., Fung, I., Miyoshi, T., & Ide, K. (2011). “Variable localization” in an ensemble Kalman filter: Application to the carbon cycle data assimilation. *Journal of Geophysical Research*, 116(D9), D09110. <https://doi.org/10.1029/2010JD014673>
- Kotsuki, S., Miyoshi, T., Terasaki, K., Lien, G.-Y., & Kalnay, E. (2017). Assimilating the global satellite mapping of precipitation data with the Nonhydrostatic Icosahedral Atmospheric Model (NICAM). *Journal of Geophysical Research: Atmosphere*, 122(2), 631–650. <https://doi.org/10.1002/2016JD025355>
- Kotsuki, S., Ota, Y., & Miyoshi, T. (2017). Adaptive covariance relaxation methods for ensemble data assimilation: Experiments in the real atmosphere. *Quarterly Journal of the Royal Meteorological Society*, 143(705). <https://doi.org/10.1002/qj.3060>
- Lacour, J.-L., Risi, C., Worden, J., Clerbaux, C., & Coheur, P.-F. (2018). Importance of depth and intensity of convection on the isotopic composition of water vapor as seen from IASI and TES δD observations. *Earth and Planetary Science Letters*, 481, 387–394. <https://doi.org/10.1016/j.epsl.2017.10.048>
- Lorenz, E. N. (1963). Deterministic nonperiodic flow. *Journal of the Atmospheric Sciences*, 20(2), 130–141. [https://doi.org/10.1175/1520-0469\(1963\)020<0130:DNF>2.0.CO;2](https://doi.org/10.1175/1520-0469(1963)020<0130:DNF>2.0.CO;2)
- Miyoshi, T. (2011). The gaussian approach to adaptive covariance inflation and its implementation with the local ensemble transform kalman filter. *Monthly Weather Review*, 139(5), 1519–1535. <https://doi.org/10.1175/2010MWR3570.1>
- Miyoshi, T., Kondo, K., & Terasaki, K. (2015). Big ensemble data assimilation in numerical weather prediction. *Computer*, 48(11), 15–21. <https://doi.org/10.1109/MC.2015.332>
- Noone, D. (2012). Pairing measurements of the water vapor isotope ratio with humidity to deduce atmospheric moistening and dehydration in the tropical midtroposphere. *Journal of Climate*, 25(13), 4476–4494. <https://doi.org/10.1175/JCLI-D-11-00582.1>
- Risi, C., Noone, D., Worden, J., Frankenberg, C., Stiller, G., Kiefer, M., et al. (2012). Process-evaluation of tropospheric humidity simulated by general circulation models using water vapor isotopologues: 1. Comparison between models and observations. *Journal of Geophysical Research*, 117(D5). <https://doi.org/10.1029/2011JD016621>
- Saunders, R., Hocking, J., Turner, E., Rayer, P., Rundle, D., Brunel, P., et al. (2018). An update on the RTTOV fast radiative transfer model (currently at version 12). *Geoscientific Model Development*, 11(7), 2717–2737. <https://doi.org/10.5194/gmd-11-2717-2018>
- Sawada, Y., Nakaegawa, T., & Miyoshi, T. (2018). Hydrometeorology as an inversion problem: Can river discharge observations improve the atmosphere by ensemble data assimilation? *Journal of Geophysical Research: Atmosphere*, 123(2), 848–860. <https://doi.org/10.1002/2017JD027531>
- Schneider, M., Borger, C., Wiegeler, A., Hase, F., García, O. E., Sepúlveda, E., & Werner, M. (2017). MUSICA MetOp/IASI {H₂O, δD} pair retrieval simulations for validating tropospheric moisture pathways in atmospheric models. *Atmospheric Measurement Techniques*, 10(2), 507–525. <https://doi.org/10.5194/amt-10-507-2017>
- Schneider, M., Wiegeler, A., Barthlott, S., González, Y., Christner, E., Dyroff, C., et al. (2016). Accomplishments of the MUSICA project to provide accurate, long-term, global and high-resolution observations of tropospheric {H₂O, δD} pairs – a review. *Atmospheric Measurement Techniques*, 9(7), 2845–2875. <https://doi.org/10.5194/amt-9-2845-2016>
- Schneider, M., Yoshimura, K., Hase, F., & Blumenstock, T. (2010). The ground-based FTIR network’s potential for investigating the atmospheric water cycle. *Atmospheric Chemistry and Physics*, 10(7), 3427–3442. <https://doi.org/10.5194/acp-10-3427-2010>
- Sherwood, S. C., Bony, S., & Dufresne, J.-L. (2014). Spread in model climate sensitivity traced to atmospheric convective mixing. *Nature*, 505(7481), 37–42. <https://doi.org/10.1038/nature12829>
- Takemi, T., Hirayama, O., & Liu, C. (2004). Factors responsible for the vertical development of tropical oceanic cumulus convection. *Geophysical Research Letters*, 31(11). <https://doi.org/10.1029/2004GL020225>
- Tardif, R., Hakim, G. J., & Snyder, C. (2015). Coupled atmosphere–ocean data assimilation experiments with a low-order model and CMIP5 model data. *Climate Dynamics*, 45(5–6), 1415–1427. <https://doi.org/10.1007/s00382-014-2390-3>
- Torn, R. D. (2010). Performance of a mesoscale Ensemble Kalman Filter (EnKF) during the NOAA high-resolution hurricane test. *Monthly Weather Review*, 138(12), 4375–4392. <https://doi.org/10.1175/2010MWR3361.1>
- Torri, G., Ma, D., & Kuang, Z. (2017). Stable water isotopes and large-scale vertical motions in the tropics. *Journal of Geophysical Research: Atmosphere*, 122(7), 3703–3717. <https://doi.org/10.1002/2016JD026154>
- Uemura, R., Matsui, Y., Yoshimura, K., Motoyama, H., & Yoshida, N. (2008). Evidence of deuterium excess in water vapor as an indicator of ocean surface conditions. *Journal of Geophysical Research*, 113(D19), D19114. <https://doi.org/10.1029/2008JD010209>
- Whitaker, J. S., & Hamill, T. M. (2012). Evaluating methods to account for system errors in ensemble data assimilation. *Monthly Weather Review*, 140(9), 3078–3089. <https://doi.org/10.1175/MWR-D-11-00276.1>
- Worden, J., Noone, D., & Bowman, K. (2007). Importance of rain evaporation and continental convection in the tropical water cycle. *Nature*, 445(7127), 528–532. <https://doi.org/10.1038/nature05508>
- Yoshimura, K. (2015). Stable water isotopes in climatology, meteorology, and hydrology: A review. *Journal of the Meteorological Society of Japan*, 93(5), 513–533. <https://doi.org/10.2151/jmsj.2015-036>
- Yoshimura, K., Frankenberg, C., Lee, J., Kanamitsu, M., Worden, J., & Röckmann, T. (2011). Comparison of an isotopic atmospheric general circulation model with new quasi-global satellite measurements of water vapor isotopologues. *Journal of Geophysical Research*, 116(D19), D19118. <https://doi.org/10.1029/2011JD016035>
- Yoshimura, K., Kanamitsu, M., Noone, D., & Oki, T. (2008). Historical isotope simulation using Reanalysis atmospheric data. *Journal of Geophysical Research*, 113(D19), D19108. <https://doi.org/10.1029/2008JD010074>
- Yoshimura, K., Miyoshi, T., & Kanamitsu, M. (2014). Observation system simulation experiments using water vapor isotope information. *Journal of Geophysical Research: Atmosphere*, 119(13), 7842–7862. <https://doi.org/10.1002/2014JD021662>
- Zhang, J., Reid, J. S., Westphal, D. L., Baker, N. L., & Hyer, E. J. (2008). A system for operational aerosol optical depth data assimilation over global oceans. *Journal of Geophysical Research*, 113(D10), D10208. <https://doi.org/10.1029/2007JD009065>

References From the Supporting Information

- Anderson, J. L. (2009). Spatially and temporally varying adaptive covariance inflation for ensemble filters. *Tellus A*, *61*(1), 72–83. <https://doi.org/10.1111/j.1600-0870.2008.00361.x>
- Hamill, T. M., Whitaker, J. S., & Snyder, C. (2001). Distance-dependent filtering of background error covariance estimates in an ensemble Kalman filter. *Monthly Weather Review*, *129*(11), 2776–2790. [https://doi.org/10.1175/1520-0493\(2001\)129<2776:DDFOBE>2.0.CO;2](https://doi.org/10.1175/1520-0493(2001)129<2776:DDFOBE>2.0.CO;2)
- Holton, J. R., & Hakim, G. J. (2013). An introduction to dynamic meteorology. *Elsevier*. <https://doi.org/10.1016/C2009-0-63394-8>
- Houtekamer, P. L., & Zhang, F. (2016). Review of the ensemble kalman filter for atmospheric data assimilation. *Monthly Weather Review*, *144*(12), 4489–4532. <https://doi.org/10.1175/MWR-D-15-0440.1>
- Miyoshi, T., Kondo, K., & Imamura, T. (2014). The 10,240-member ensemble Kalman filtering with an intermediate AGCM. *Geophysical Research Letters*, *41*(14), 5264–5271. <https://doi.org/10.1002/2014GL060863>
- Miyoshi, T., & Yamane, S. (2007). Local ensemble transform kalman filtering with an AGCM at a T159/L48 resolution. *Monthly Weather Review*, *135*(11), 3841–3861. <https://doi.org/10.1175/2007MWR1873.1>
- Wilks, D. S. (2019). Statistical methods in the atmospheric sciences. *Elsevier*. <https://doi.org/10.1016/C2017-0-03921-6>
- Yanai, M., Esbensen, S., & Chu, J.-H. (1973). Determination of bulk properties of tropical cloud clusters from large-scale heat and moisture budgets. *Journal of the Atmospheric Sciences*, *30*(4), 611–627. [https://doi.org/10.1175/1520-0469\(1973\)030<0611:DOBPOT>2.0.CO;2](https://doi.org/10.1175/1520-0469(1973)030<0611:DOBPOT>2.0.CO;2)
- Yu, B., & Boer, G. J. (2002). The roles of radiation and dynamical processes in the El Niño-like response to global warming. *Climate Dynamics*, *19*(5–6), 539–554. <https://doi.org/10.1007/s00382-002-0244-x>